

Constraints on scalar and vector leptoquarks from the LHC Higgs data

Jian Zhang ^{a1} Chong-Xing Yue ^{a2} Chun-Hua Li ^a and Shuo Yang ^b

^aDepartment of Physics, Liaoning Normal University, Dalian 116029, China

^bDepartment of Physics, Dalian University, Dalian 116622, China

Abstract

We study contributions of single scalar or vector leptoquark (LQ) to loop-induced Higgs processes, gluon fusion production ($gg \rightarrow h$) and $h \rightarrow \gamma\gamma$ decay, by analyzing the current Higgs data from the LHC Run I and II. Scalar LQ is studied in a model independent way, while the vector LQ $U_1(\mathbf{3}, \mathbf{1}, 2/3)$ is discussed in the '4321' model. Constraints on the interactions of LQ and Higgs boson are obtained. We provide a method to determine vacuum expectation values v_3 and v_1 of the new scalar fields Ω_3 and Ω_1 in the '4321' model via the combination of Higgs data and measurements of $R_{D^{(*)}}$ and $R_{K^{(*)}}$.

¹E-mail: zhangjianphy@aliyun.com

²E-mail: cxyue@lnnu.edu.cn

1 Introduction

In the last few years accumulated experimental results of semileptonic B -meson decays point to lepton flavour universality violation (LFUV). In the case of flavor changing neutral current (FCNC) transition $b \rightarrow s\mu^+\mu^-$, ratios $R_{K^{(*)}} = \frac{\mathcal{B}(\bar{B} \rightarrow K^{(*)}\mu^+\mu^-)}{\mathcal{B}(\bar{B} \rightarrow K^{(*)}e^+e^-)}$ measured by the LHCb collaboration are lower than the SM expectations by $\sim 2.6\sigma$ [1–4]. For $b \rightarrow c\ell\nu$ ($\ell = e, \mu$) charged current case, measurements of $R_D = \frac{\mathcal{B}(\bar{B} \rightarrow D\tau^-\bar{\nu})}{\mathcal{B}(\bar{B} \rightarrow D\ell^-\bar{\nu})}$ and $R_{D^*} = \frac{\mathcal{B}(\bar{B} \rightarrow D^*\tau^-\bar{\nu})}{\mathcal{B}(\bar{B} \rightarrow D^*\ell^-\bar{\nu})}$ from experiments are higher than the SM expectations by $\sim 2.3\sigma$ and $\sim 3.4\sigma$, respectively [5–13]. As popular candidates for explaining B -anomalies, leptoquarks (LQs) are extensively discussed in specific ultraviolet (UV) theories or model-independently (see, e.g, [14–51]).

LQs are hypothetical color-triplet bosons that carry both baryon and lepton numbers [52–54]. They naturally appear in many extensions of the Standard Model (SM) such as Pati-Salam model [55], grand unification theories based on $SU(5)$ [56] and $SO(10)$ [57], extended technicolor [58], and compositeness [59]. According to their properties under the Lorentz transformations, LQs can be either scalar (spin 0) or vector (spin 1). Several models suggest LQs mass of TeV-scale.

LQs can also couple to Higgs boson and considerably modify loop-induced Higgs processes, gluon fusion production (ggF) and $h \rightarrow \gamma\gamma$ decay, without appreciably changing kinematics of these processes. Scalar LQs interact with the Higgs boson at tree level via Higgs portal interactions. Their contributions to loop-induced Higgs processes can be studied model-independently [53, 60, 61]. Vector LQs, as gauge fields in full fledged models, make contributions to the loop processes that are sensitive to the gauge sector of the ultraviolet (UV) theories which they belong to. ggF predominates the Higgs production processes at the LHC. And the LHC is sensitive to $h \rightarrow \gamma\gamma$ decay process. After the discovery of the 125 GeV Higgs boson by the ATLAS [62] and CMS [63] experiments in 2012, precisely measuring properties of the Higgs boson are then performed by the ATLAS and CMS experiments with LHC Run I and II data sets [64–66]. Globally analyzing these measurements, in some sense, can guide us for LQs study.

Constraints on scalar LQs are obtained by Ref. [53] via analyzing Higgs data from the LHC Run I reported by the ATLAS and CMS collaborations [67, 68]. We update these results via comprehensively analyzing Higgs data from the LHC Run I and II [64–66].

Since interactions between vector LQ and the Higgs boson as well as other gauge fields are sensitive to the UV theories which the LQ belongs to, the contributions of vector LQ to the loop-induced Higgs processes should be studied in a specific model. Of particular note is that $U_1(\mathbf{3}, \mathbf{1}, 2/3)$ with mass of several TeV performs quite well in explaining both anomalies of $R_{D^{(*)}}$ and $R_{K^{(*)}}$ [19]. In this article, we study $U_1(\mathbf{3}, \mathbf{1}, 2/3)$ originating from a particular theory, namely the '4321' model. One of purposes of the model is to explain B -anomalies [21, 31]. Besides obtaining the constraints on the size of vector LQ interactions to the Higgs boson from current LHC Higgs data, we also provide a method to determine vacuum expectation values (VEVs) v_3 and v_1 of the new scalar fields Ω_3 and Ω_1 in the '4321' model via the combination of Higgs data and measurements of $R_{D^{(*)}}$ and $R_{K^{(*)}}$.

The article is organized as follows: we first review current Higgs data from the LHC Run I and II in Section 2. In Section 3, we model-independently study the contributions of single scalar LQ to loop-induced Higgs processes, ggF production and $h \rightarrow \gamma\gamma$ decay. Contributions of the vector LQ U_1 to these loop processes are discussed in framework of the '4321' model in Section 4. In the same

section, we also discuss the determination of VEVs v_3 and v_1 of this model. Finally, conclusions for this work are given in Section 5.

2 The LHC Higgs data

The discovery of the 125 GeV Higgs boson by the ATLAS [62] and CMS [63] experiments in 2012 is one of the greatest achievements in the history of particle physics. Precise measurements of the Higgs boson properties are then performed by these experiments. At the LHC, only products of cross sections and branching fractions are measured. In the narrow-width approximation, the signal cross section of an individual channel, e.g. $\sigma(gg \rightarrow H \rightarrow \gamma\gamma)$, can be factorized as [69]

$$\begin{aligned} \sigma(gg \rightarrow H \rightarrow \gamma\gamma) &= \frac{\sigma_{ggF} \cdot \Gamma^{\gamma\gamma}}{\Gamma_h} \\ &= (\sigma_{ggF} \cdot B^{\gamma\gamma})_{SM} \frac{\kappa_g^2 \cdot \kappa_\gamma^2}{\kappa_h^2}, \end{aligned} \quad (1)$$

where σ_i and Γ^j represent measured values of $i \rightarrow h$ production and $h \rightarrow j$ decay, respectively, and σ_i^{SM} and Γ_{SM}^j are their SM expectations, κ_i are the so called 'coupling modifiers' defined as $\kappa_i^2 = \sigma_i/\sigma_i^{SM}$ or $\kappa_i^2 = \Gamma^i/\Gamma_{SM}^i$ (all κ_i values equal unity in the SM), and Γ_h denotes the total width of the Higgs boson.

In 2016, the ATLAS and CMS collaborations reported measurements of the Higgs boson production and decay rates as well as constraints on its couplings to vector bosons and fermions by using the LHC Run I data recorded in 2011 and 2012 [64]. The integrated luminosities in each experiment are about 5 fb^{-1} at $\sqrt{s} = 7 \text{ TeV}$ and 20 fb^{-1} at $\sqrt{s} = 8 \text{ TeV}$. The measurements are based on five main Higgs boson production processes (gluon fusion, vector boson fusion, and associated production with a W or a Z boson or pair of top quarks) and six decay modes ($h \rightarrow ZZ, WW, \gamma\gamma, \tau\tau, bb$ and $\mu\mu$).

In 2019, the similar measurements are reported by the ATLAS and CMS collaborations via using the Run II data set recorded by the ATLAS detector during 2015, 2016 and 2017 with the integrated luminosity of 79.8 fb^{-1} at $\sqrt{s} = 13 \text{ TeV}$ [65] and the CMS detector in 2016 at $\sqrt{s} = 13 \text{ TeV}$ with the integrated luminosity of 35.9 fb^{-1} [66], respectively.

The Higgs boson with mass of $m_h = 125.09 \text{ GeV}$ is assumed in all the above experimental analyses. These measurements normalized to the SM predictions are listed in Table 1. From Table 1 we can see that measurements obtained by each experiment from the LHC Run I or Run II are precisely consistent within error with their SM predictions. This implies that NP properly lies in a scale much higher than the mass of Higgs boson, and new heavy particles carrying electric and colour charge may still be present in the loop-induced Higgs processes, ggF production and $h \rightarrow \gamma\gamma$ decay, without appreciably changing kinematics of these process [61, 70–75].

To test our point of view, we perform a fit to these measurements by minimizing a χ^2 function, which is defined as

$$\chi_{\text{Higgs}}^2 = \sum_{i=1}^{28} \sum_{j=1}^{28} [E_i - T_i] C_{ij}^{-1} [E_j - T_j], \quad (2)$$

where E_i denotes experimentally measured $\sigma_{ggF} \cdot B_{ZZ}$, σ_i/σ_{ggF} or $\mathcal{B}_i/\mathcal{B}_{ZZ}$ and T_i is its theoretical expectation. C is a 28×28 covariance matrix, which can be constructed by using the standard

Table 1: Best fit values of $\sigma(gg \rightarrow h \rightarrow ZZ)$, σ_i/σ_{ggF} and $\mathcal{B}^f/\mathcal{B}^{ZZ}$ obtained from different experiments. The measurements are normalized to the SM predictions.

Measurements	Values		
	ATLAS & CMS [64]	ATLAS [65]	CMS [66]
	$\sqrt{s} = 8$ TeV	$\sqrt{s} = 13$ TeV	$\sqrt{s} = 13$ TeV
$\sigma_{ggF} \cdot B_{ZZ}$	$1.16^{+0.26}_{-0.24}$	$1.13^{+0.13}_{-0.13}$	$1.07^{+0.20}_{-0.18}$
$\sigma_{VBF}/\sigma_{ggF}$	$1.33^{+0.44}_{-0.36}$	$1.23^{+0.32}_{-0.27}$	$0.6^{+0.30}_{-0.24}$
σ_{WH}/σ_{ggF}	$0.84^{+0.76}_{-0.71}$	$1.26^{+0.59}_{-0.45}$	$2.19^{+0.86}_{-0.69}$
σ_{ZH}/σ_{ggF}	$3.06^{+1.84}_{-1.48}$	$1.01^{+0.47}_{-0.35}$	$0.88^{+0.34}_{-0.27}$
$\sigma_{ttH\ddagger tH}/\sigma_{ggF}$	$3.28^{+1.15}_{-1.02}$	$1.20^{+0.31}_{-0.27}$	$1.06^{+0.34}_{-0.27}$
$\mathcal{B}_{\gamma\gamma}/\mathcal{B}_{ZZ}$	$0.81^{+0.21}_{-0.16}$	$0.87^{+0.14}_{-0.12}$	$1.14^{+0.28}_{-0.20}$
$\mathcal{B}_{WW}/\mathcal{B}_{ZZ}$	$0.83^{+0.20}_{-0.16}$	$0.85^{+0.18}_{-0.15}$	$1.23^{+0.27}_{-0.22}$
$\mathcal{B}_{\tau\tau}/\mathcal{B}_{ZZ}$	$0.76^{+0.26}_{-0.21}$	$0.86^{+0.26}_{-0.22}$	$1.07^{+0.37}_{-0.30}$
$\mathcal{B}_{bb}/\mathcal{B}_{ZZ}$	$0.20^{+0.21}_{-0.12}$	$0.93^{+0.38}_{-0.28}$	$0.84^{+0.37}_{-0.27}$
$\mathcal{B}_{\mu\mu}/\mathcal{B}_{ZZ}$	—	—	$0.63^{+1.24}_{-1.21}$

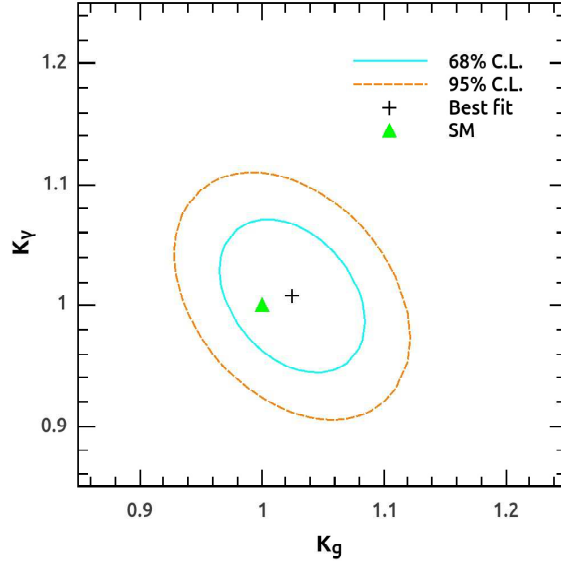


Figure 1: Two dimensional likelihood contours at 68% and 95% C.L. in $(\kappa_g, \kappa_\gamma)$ plane obtained from the LHC Run I and Run II Higgs data. The cross and triangle are the best-fit value and SM prediction, respectively.

errors and corresponding correlations between these measurements obtained from the original articles published.

Assuming that BSM contributes to the loop processes only, we have

$$\kappa_h^2 = \frac{\Gamma_h}{\Gamma_h^{SM}}. \quad (3)$$

In this case, the coupling modifiers κ_γ and κ_g are free and other κ_i are fixed to unity. The best fit to the measurements yields

$$\kappa_\gamma = 1.008 \pm 0.042, \quad \kappa_g = 1.025 \pm 0.040, \quad (4)$$

with the correlation between the two quantities $\rho = -0.34$. Two dimensional likelihood contours at 68% and 95% C.L. in $(\kappa_g, \kappa_\gamma)$ plane are shown in Fig. 1. The fitting results are in good agreement within error with the SM predictions (errors of κ_γ and κ_g are both reduced to about 4%), which further support our argument of NP only modifying loop-induced Higgs processes.

The appropriate cumulative distribution functions are used to obtain the upper bounds for this and following analysis, namely, 68% (95%) best-fit region satisfies $\chi^2 - \chi_{min}^2 \leq 0.99$ (3.84) for one parameter, and $\chi^2 - \chi_{min}^2 \leq 2.28$ (5.99) for two parameters.

3 Scalar LQs

By using transformations under the SM gauge group $\mathcal{G}_{SM} = SU(3)_c \times SU(2)_L \times U(1)_Y$ as the classification criterion, there are six possible scalar LQ multiplets [53]: $S_3(\mathbf{\bar{3}}, \mathbf{3}, 1/3)$, $R_2(\mathbf{3}, \mathbf{2}, 7/6)$, $\tilde{R}_2(\mathbf{3}, \mathbf{2}, 1/6)$, $\tilde{S}_1(\mathbf{\bar{3}}, \mathbf{1}, 4/3)$, $S_1(\mathbf{\bar{3}}, \mathbf{1}, 1/3)$, $\bar{S}_1(\mathbf{\bar{3}}, \mathbf{1}, -2/3)$. The first number, the second one and the last one within each brackets indicates the QCD representation, the weak isospin representation and the weak hypercharge, respectively.

The colorless vacuum requires that these colored scalars cannot acquire their masses via spontaneous symmetry breaking [61]. Assuming weak components of single scalar LQ multiplet (S) to be degenerate at the electroweak scale, namely the mass of scalar LQ, m_S , is a free parameter, the Higgs portal interaction reads [53]

$$\mathcal{L} \ni -\lambda_S (S_{ia}^\dagger S_{ia})(H_j^\dagger H_j) = -\lambda_S v (S_{ia}^\dagger S_{ia}) h, \quad (5)$$

where i, j are weak indices, a represents color index, λ_S is the coupling constant for the LQ-Higgs-LQ vertex, v is vacuum expectation of the Higgs boson with $v = 246.22$ GeV.

Contributions of S to loop-induced Higgs processes arise from Eq. (5), and are described by only two independent parameters, λ_S and m_S . For convenience, a new parameter $\xi_S(\lambda_S, m_S^2) \equiv \lambda_S(v/m_S)^2$ is introduced.

In the SM, W boson and top quark loops dominate the partial decay width of $h \rightarrow \gamma\gamma$ decay. The partial decay width in presence of single scalar LQ S is given by

$$\Gamma(h \rightarrow \gamma\gamma) = \frac{G_F \alpha_{em}^2 m_h^3}{128 \sqrt{2} \pi^3} \left| F_1(x_W) + \frac{4}{3} F_{1/2}(x_t) + \sum_i \frac{\xi_S}{2} d(r_S) Q_{S_i}^2 F_0(x_S) \right|^2, \quad (6)$$

where G_F and α_{em} are the Fermi and fine-structure constants, respectively, Q_{S_i} is electric charge of the weak component S_i of single representation S , the sum of i is taken over the weak components, $d(r_S)$ represents the dimension of the color representation, and $x_i \equiv m_h^2/(4m_i^2)$ ($i = W, t, S$). The one-loop functions $F(x)$ read

$$\begin{aligned} F_1(x) &= [x(2x+3) + 3(2x-1)f(x)] x^{-2}, \\ F_{1/2}(x) &= -2[x + (x-1)f(x)] x^{-2}, \\ F_0(x) &= [x - f(x)] x^{-2}, \end{aligned} \quad (7)$$

with the function

$$f(x) = \begin{cases} \arcsin^2 \sqrt{x} & x \leq 1 \\ -\frac{1}{4} \left(\log \frac{1+\sqrt{1-x^{-1}}}{1-\sqrt{1-x^{-1}}} - i\pi \right)^2 & x < 1 \end{cases}. \quad (8)$$

Then, one can obtain normalized modification of partial decay width of $h \rightarrow \gamma\gamma$ decay induced by single scalar LQ, which is expressed as [53]

$$\frac{\Gamma_{h \rightarrow \gamma\gamma}}{\Gamma_{h \rightarrow \gamma\gamma}^{SM}} = |\kappa_\gamma|^2, \text{ where } \kappa_\gamma = 1 - 0.026\xi_S d(r_S) \sum_i Q_{S_i}^2. \quad (9)$$

In the SM, top quark loop dominates the ggF Higgs production cross section. In presence of single scalar LQ S , the leading order parton cross section of $gg \rightarrow h$ at the partonic center mass of energy $\sqrt{\hat{s}}$ can be expressed as

$$\hat{\sigma}_{LO}(gg \rightarrow h) = \frac{\sigma_0}{m_h^2} \delta(\hat{s} - m_h^2), \quad (10)$$

where σ_0 is proportional to the partial decay width of $h \rightarrow gg$ decay, which is given by

$$\begin{aligned} \sigma_0 &= \frac{8\pi^2}{m_h^3} \Gamma_{LO}(h \rightarrow gg) \\ &= \frac{G_F \alpha_s^2(\mu^2)}{512\sqrt{2}\pi} \left| F_{1/2}(x_t) + \sum_i^{N_{S_i}} \xi_S C(r_S) F_0(x_S) \right|^2, \end{aligned} \quad (11)$$

where $\alpha_s^2(\mu^2)$ represents the strong coupling constant, F_0 term induced by single scalar LQ S . $C(r_S)$ is the index of color representation of S ($C(r_S) = 1/2$ for color triplet) and N_{S_i} is the number of weak components of S . Effects of higher order QCD are neglected, since the ratio, $\sigma/(\sigma)_{SM}$, is found to be less sensitive to that [75]. The normalized modification of ggF Higgs production cross section induced by single scalar LQ is given by [53]

$$\frac{\sigma_{gg \rightarrow h}}{\sigma_{gg \rightarrow h}^{SM}} = |\kappa_g|^2, \text{ where } \kappa_g = 1 + 0.24\xi_S N_{S_i} C(r_S). \quad (12)$$

Thus for the case of single scalar LQ representation S modifies the loop-induced Higgs processes, there is only one free parameter ξ_S left.

To obtain ξ_S , we re-perform the Higgs fit by using ξ_S to replace κ_γ and κ_g via Eqs. (9) and (12). Best values of ξ_S with standard errors and 95% C.L. intervals for all six scalar LQ representations are shown in Table 2. Errors of ξ_S for all scalar LQs obtained in this analysis are reduced more than half compared with previous analysis in Ref. [53]. But constraints on ξ_S for all scalar LQs are still too loose to acquire exact information for scalar LQs with TeV-scale masses. Table 3 shows best values of scalar LQs masses and their lower limits at 95% C.L. in the assumption of the portal coupling $\lambda_S = 1.0$. If LQs are insensitive to generation as well as their decay modes, the most stringent limits on the mass of scalar LQs reads $m_S > 1560$ GeV reported by the ATLAS collaboration [76]. Assuming $m_S = 1560$ GeV, best values of portal couplings λ_S and their upper limits at 95% C.L. obtained from Higgs fit are shown in Table 4.

Table 2: Constraints on LQs from the LHC Run I and II Higgs data for all scalar LQ representations, where $\xi_S = \lambda_S v^2 / m_S^2$.

Scalar LQ	$\xi_S = \lambda_S v^2 / m_S^2$	
	best fit	95% C.L.
$S_3(\mathbf{3}, \mathbf{3}, 1/3)$	0.060 ± 0.108	$[-0.173, 0.294]$
$R_2(\mathbf{3}, \mathbf{2}, 7/6)$	0.032 ± 0.134	$[-0.241, 0.326]$
$\tilde{R}_2(\mathbf{3}, \mathbf{2}, 1/6)$	0.115 ± 0.162	$[-0.237, 0.456]$
$\tilde{S}_1(\mathbf{3}, \mathbf{1}, 4/3)$	0.048 ± 0.245	$[-0.465, 0.604]$
$S_1(\mathbf{3}, \mathbf{1}, 1/3)$	0.234 ± 0.316	$[-0.452, 0.895]$
$\bar{S}_1(\mathbf{3}, \mathbf{1}, -2/3)$	0.220 ± 0.329	$[-0.494, 0.917]$

Table 3: For the LQ-Higgs coupling $\lambda_S = 1.0$, best values and lower limits at 95% C.L. of scalar LQs masses obtained from Higgs fit.

Scalar LQ	$m_S (\lambda_S = 1.0)$	
	best fit	95% C.L.
$S_3(\mathbf{3}, \mathbf{3}, 1/3)$	1005 GeV	> 454 GeV
$R_2(\mathbf{3}, \mathbf{2}, 7/6)$	1376 GeV	> 431 GeV
$\tilde{R}_2(\mathbf{3}, \mathbf{2}, 1/6)$	726 GeV	> 364 GeV
$\tilde{S}_1(\mathbf{3}, \mathbf{1}, 4/3)$	1124 GeV	> 317 GeV
$S_1(\mathbf{3}, \mathbf{1}, 1/3)$	509 GeV	> 260 GeV
$\bar{S}_1(\mathbf{3}, \mathbf{1}, -2/3)$	525 GeV	> 257 GeV

The results are expected to be significantly improved at High Luminosity (HL)-LHC. Ref. [77] reported the projections for Higgs couplings determinations at HL-LHC with an integrated luminosity of 3000 fb^{-1} . The precision on κ_γ and κ_g is expected to be 2.4% and 3.1% at the ATLAS experiment while that is 2.0% and 2.5% at the CMS experiment. Thus the precision on κ_γ and κ_g is expected to be 1.5% and 1.9% at HL-LHC by combining the ATLAS and CMS measurements of κ_γ and κ_g . Then we can obtain the precision on ξ_S expected at the HL-LHC via Eqs. (9) and (12). The approximate relation between errors of ξ_S and κ_γ and κ_g read

$$\delta_{\xi_S} \approx \left[0.24 N_{S_i} C(r_S) - 0.026 d(r_S) \sum_i Q_{S_i}^2 \right] \sqrt{\delta_{\kappa_g}^2 + \delta_{\kappa_\gamma}^2}. \quad (13)$$

Compared to the present precision on ξ_S , the situation is expected to improve by a factor of 2.4 at the HL-LHC.

4 Vector LQ $U_1(\mathbf{3}, \mathbf{1}, 2/3)$ in the '4321' model

Now we consider contributions of vector LQ $U_1(\mathbf{3}, \mathbf{1}, 2/3)$ to the loop-induced Higgs processes $gg \rightarrow h$ and $h \rightarrow \gamma\gamma$, which LQ performs quite well in explaining both anomalies of $R_{D^{(*)}}$ and $R_{K^{(*)}}$. Our

Table 4: For $m_S = 1000$ GeV, best values and upper limits at 95% C.L. of the size of LQ-Higgs coupling $|\lambda_S|$ for scalar LQs obtained from Higgs fit.

Scalar LQ	λ_S ($m_S = 1560$ GeV)	
	best fit	95% C.L.
$S_3(\mathbf{\bar{3}}, \mathbf{3}, 1/3)$	2.4	< 11.8
$R_2(\mathbf{3}, \mathbf{2}, 7/6)$	1.3	< 13.1
$\tilde{R}_2(\mathbf{3}, \mathbf{2}, 1/6)$	4.6	< 18.3
$\tilde{S}_1(\mathbf{\bar{3}}, \mathbf{1}, 4/3)$	1.9	< 24.2
$S_1(\mathbf{\bar{3}}, \mathbf{1}, 1/3)$	9.4	< 35.9
$\bar{S}_1(\mathbf{\bar{3}}, \mathbf{1}, -2/3)$	8.8	< 36.8

study in framework of the '4321' model [21, 31]. We first briefly review the '4321' model, then we study contributions of U_1 to the loop-induced Higgs processes. Constraints on the interactions of U_1 with the Higgs boson from LHC Higgs data is obtained. Further more, we obtain constraints on the VEVs v_3 and v_1 of new scalar fields Ω_3 and Ω_1 in the model.

4.1 The '4321' model

The model gauge group is expressed as $\mathcal{G}_{4321} = SU(4) \times SU(3)' \times SU(2)_L \times U(1)'$, for which $H_\mu^\alpha, G_\mu^a, W_\mu^i, B_\mu'$ denote corresponding gauge fields, g_4, g_3, g_2, g_1 the gauge couplings and T^α, T^a, T^i, Y' the generators, where the indices $\alpha = 1, \dots, 15$, $a = 1, \dots, 8$, $i = 1, \dots, 3$. The generators are normalized in such a way that $\text{Tr} T^A T^B = \frac{1}{2} \delta^{AB}$. The SM gauge symmetry $SU(3)_c \times U(1)_Y$ is embedded in $SU(4) \times SU(3)' \times U(1)'$.

The model comprises four scalar representations: $\Omega_3(\bar{\mathbf{4}}, \mathbf{3}, \mathbf{1}, 1/6)$, $\Omega_1(\bar{\mathbf{4}}, \mathbf{1}, \mathbf{1}, -1/2)$, $\Omega_{15}(\bar{\mathbf{15}}, \mathbf{1}, \mathbf{1}, 0)$ and $\Phi(\mathbf{1}, \mathbf{1}, \mathbf{2}, 1/2)$, where Ω_3 and Ω_1 are respectively a 4×3 matrix and a 4-vector transforming as $\Omega_3 \rightarrow U_4^* \Omega_3 U_3^T$ and $\Omega_1 \rightarrow U_4^* \Omega_1$ under $SU(4) \times SU(3)'$ and H is the Higgs doublet (in this analysis we neglect the effect of Ω_{15}). Phenomenological considerations suggest : $\langle \Omega_3 \rangle > \langle \Omega_1 \rangle > \langle \Phi \rangle$. According to Ref. [31], the most general scalar potential involving $\Omega_{3,1}$ and H can be written as

$$\begin{aligned}
V = & + \mu_3^2 \text{Tr}(\Omega_3^\dagger \Omega_3) + \lambda_1 \left(\text{Tr}(\Omega_3^\dagger \Omega_3) - \frac{3}{2} v_3^2 \right)^2 + \lambda_2 \text{Tr} \left(\Omega_3^\dagger \Omega_3 - \frac{1}{2} v_3^2 \right)^2 \\
& + \mu_1^2 |\Omega_1|^2 + \lambda_3 \left(|\Omega_1|^2 - \frac{1}{2} v_1^2 \right)^2 + \lambda_4 \left(\text{Tr}(\Omega_3^\dagger \Omega_3) - \frac{3}{2} v_3^2 \right) \left(|\Omega_1|^2 - \frac{1}{2} v_1^2 \right) \\
& + \lambda_5 \Omega_1^\dagger \Omega_3 \Omega_3^\dagger \Omega_1 + \lambda_6 ([\Omega_3 \Omega_3 \Omega_3 \Omega_1]_1 + \text{h.c.}) + \mu_\Phi^2 \Phi^\dagger \Phi + \lambda_7 \left(\Phi^\dagger \Phi - \frac{v^2}{2} \right)^2 \\
& + \lambda_8 \left(\text{Tr}(\Omega_3^\dagger \Omega_3) - \frac{3}{2} v_3^2 \right) \left(\Phi^\dagger \Phi - \frac{v^2}{2} \right) + \lambda_9 \left(|\Omega_1|^2 - \frac{1}{2} v_1^2 \right) \left(\Phi^\dagger \Phi - \frac{v^2}{2} \right). \quad (14)
\end{aligned}$$

where $[\Omega_3\Omega_3\Omega_3\Omega_1]_1 \equiv \epsilon_{\alpha\beta\gamma\delta}\epsilon^{abc}(\Omega_3)_a^\alpha(\Omega_3)_b^\beta(\Omega_3)_c^\gamma(\Omega_1)^\delta$. VEV configurations [31]

$$\langle\Omega_3\rangle = \frac{1}{\sqrt{2}} \begin{pmatrix} v_3 & 0 & 0 \\ 0 & v_3 & 0 \\ 0 & 0 & v_3 \\ 0 & 0 & 0 \end{pmatrix}, \quad \langle\Omega_1\rangle = \frac{1}{\sqrt{2}} \begin{pmatrix} 0 \\ 0 \\ 0 \\ v_1 \end{pmatrix}, \quad (15)$$

together with $\mu_3^2 = -3\lambda_6 v_3 v_1$, $\mu_1^2 = -3\lambda_6 v_3^2/v_1$ and $\mu_h^2 = 0$ in Eq. (14) ensure the proper $\mathcal{G}_{4321} \rightarrow \mathcal{G}_{SM}$ breaking. Under \mathcal{G}_{SM} , Ω_3 and Ω_1 decomposed as: $\Omega_3 \rightarrow \mathbb{S}_3(\mathbf{1}, \mathbf{1}, 0) \oplus \mathbb{T}_3(\mathbf{3}, \mathbf{1}, 2/3) \oplus \mathbb{O}_3(\mathbf{8}, \mathbf{1}, 0)$ and $\Omega_1 \rightarrow \mathbb{S}_1(\mathbf{1}, \mathbf{1}, 0) \oplus \mathbb{T}_1^*(\mathbf{3}, \mathbf{1}, 2/3)$. The final breaking of \mathcal{G}_{SM} proceeds via the Higgs doublet field acquiring a VEV $\langle\Phi\rangle = (0 \ v)^T/\sqrt{2}$, with $v = 246.22$ GeV.

The covariant derivatives of Ω_3 , Ω_1 and Φ are given by

$$\begin{aligned} D_\mu\Omega_3 &= \partial_\mu\Omega_3 + ig_4 H_\mu^\alpha T^{*\alpha}\Omega_3 - ig_3 G_\mu^a T^a\Omega_3 - \frac{1}{6}ig_1 B'_\mu\Omega_3, \\ D_\mu\Omega_1 &= \partial_\mu\Omega_1 + ig_4 H_\mu^\alpha T^{*\alpha}\Omega_1 + \frac{1}{2}ig_1 B'_\mu\Omega_1, \\ D_\mu\Phi &= \partial_\mu\Phi - ig_2 W_\mu^i T^i\Phi - \frac{1}{2}ig_1 B'_\mu\Phi \end{aligned} \quad (16)$$

In the model, the mass of U_1 and corresponding mass eigenstate expressed in terms of the original gauge fields are given by [31]

$$m_U = \frac{1}{2}g_4\sqrt{v_3^2 + v_1^2}, \quad (17)$$

and

$$U_{1\mu}^{1,2,3} = \frac{1}{2}(H_\mu^{9,11,13} - iH_\mu^{10,12,14}). \quad (18)$$

Then we obtain Feynman rules of U_1 interactions to scalars

$$\begin{pmatrix} U_{1\mu} \\ U_{1\nu}^* \\ \mathbb{S}_3^{(*)} \end{pmatrix} : \frac{i}{2}g_4^2 \frac{v_3}{4\sqrt{3}} g_{\mu\nu}, \quad \begin{pmatrix} U_{1\mu} \\ U_{1\nu}^* \\ \mathbb{S}_1^{(*)} \end{pmatrix} : \frac{i}{2}g_4^2 \frac{v_1}{2\sqrt{2}} g_{\mu\nu}, \quad (19)$$

From Eq. (16) we can see that U_1 can not couple to the Higgs doublet Φ directly. U_1 interacts with the Higgs boson h via the mixing of $\phi^{(*)}$ and representations $\mathbb{S}_{3,1}^{(*)}(\mathbf{1}, \mathbf{1}, 0)$ after the final SM breaking, where ϕ represents the neutral component of the Higgs doublet and $\mathbb{S}_{3,1}(\mathbf{1}, \mathbf{1}, 0)$ are decompositions of $\Omega_{3,1}$ under the SM symmetry. In the basis $(\mathbb{S}_3, \mathbb{S}_3^*, \mathbb{S}_1, \mathbb{S}_1^*, \phi, \phi^*)$, singlet spectrum are expressed as

$$\mathcal{M}_S^2 = \begin{pmatrix} \mathcal{M}_1^2 & \mathcal{M}_2^2 & \mathcal{M}_3^2 & \frac{1}{2}\sqrt{\frac{3}{2}}\lambda_4 v_1 v_3 & \frac{1}{2}\sqrt{\frac{3}{2}}\lambda_8 v v_3 & \frac{1}{2}\sqrt{\frac{3}{2}}\lambda_8 v v_3 \\ \mathcal{M}_2^2 & \mathcal{M}_1^2 & \frac{1}{2}\sqrt{\frac{3}{2}}\lambda_4 v_1 v_3 & \mathcal{M}_3^2 & \frac{1}{2}\sqrt{\frac{3}{2}}\lambda_8 v v_3 & \frac{1}{2}\sqrt{\frac{3}{2}}\lambda_8 v v_3 \\ \mathcal{M}_3^2 & \frac{1}{2}\sqrt{\frac{3}{2}}\lambda_4 v_1 v_3 & \lambda_3 v_1^2 & \lambda_3 v_1^2 - 3\lambda_6 \frac{v_3^2}{v_1} & \frac{1}{2}\lambda_9 v v_1 & \frac{1}{2}\lambda_9 v v_1 \\ \frac{1}{2}\sqrt{\frac{3}{2}}\lambda_4 v_1 v_3 & \mathcal{M}_3^2 & \lambda_3 v_1^2 - 3\lambda_6 \frac{v_3^2}{v_1} & \lambda_3 v_1^2 & \frac{1}{2}\lambda_9 v v_1 & \frac{1}{2}\lambda_9 v v_1 \\ \frac{1}{2}\sqrt{\frac{3}{2}}\lambda_8 v v_3 & \frac{1}{2}\sqrt{\frac{3}{2}}\lambda_8 v v_3 & \frac{1}{2}\lambda_9 v v_1 & \frac{1}{2}\lambda_9 v v_1 & \lambda_7 v^2 & \lambda_7 v^2 \\ \frac{1}{2}\sqrt{\frac{3}{2}}\lambda_8 v v_3 & \frac{1}{2}\sqrt{\frac{3}{2}}\lambda_8 v v_3 & \frac{1}{2}\lambda_9 v v_1 & \frac{1}{2}\lambda_9 v v_1 & \lambda_7 v^2 & \lambda_7 v^2 \end{pmatrix}, \quad (20)$$

where

$$\mathcal{M}_1^2 = \frac{1}{2}(3\lambda_1 + \lambda_2)v_3^2 + 3\lambda_6 v_1 v_3, \quad \mathcal{M}_2^2 = \frac{1}{2}(3\lambda_1 + \lambda_2)v_3^2 - \frac{3}{2}\lambda_6 v_1 v_3, \quad \mathcal{M}_3^2 = \sqrt{\frac{3}{2}} \left(3\lambda_6 v_3^2 + \frac{1}{2}\lambda_4 v_1 v_3 \right).$$

It turns out $\mathcal{M}_5^2 = 4$. Two massless modes correspond to eigenvectors

$$S_{GB}^Z = \frac{1}{\sqrt{2}}(0, 0, 0, 0, -1, 1), \quad (21)$$

and

$$S_{GB}^{Z'} = \frac{1}{\sqrt{\frac{2}{3}v_3^2 + v_1^2}} \left(\frac{v_3}{\sqrt{3}}, -\frac{v_3}{\sqrt{3}}, -\frac{v_1}{\sqrt{2}}, \frac{v_1}{\sqrt{2}}, 0, 0 \right), \quad (22)$$

which are associated to the longitudinal degrees of freedom of the Z and Z' , respectively. One of four non-zero eigenvalues as well as corresponding eigenvector can be also easily obtained as

$$\mathcal{M}_{S_0}^2 = \frac{3\lambda_6 v_3 (2v_3^2 + 3v_1^2)}{2v_1}, \quad (23)$$

and

$$S_0 = \frac{1}{\sqrt{\frac{2}{3}v_3^2 + v_1^2}} \left(-\frac{v_1}{\sqrt{2}}, \frac{v_1}{\sqrt{2}}, -\frac{v_3}{\sqrt{3}}, \frac{v_3}{\sqrt{3}}, 0, 0 \right). \quad (24)$$

Precisely acquiring mass eigenvalue of the would-be Higgs boson and corresponding eigenvector is difficult, unless conditions such as precise value of the Higgs mass obtained from experiment as well as other constraints are applied. We assume the Higgs boson with mass value of 125.09 GeV corresponds to normalized eigenvector

$$h = (\lambda_{S_3}, \lambda_{S_3^*}, \lambda_{S_1}, \lambda_{S_1^*}, \lambda_\phi, \lambda_{\phi^*}), \quad (25)$$

where $\lambda_{S_3^{(*)}}$, $\lambda_{S_1^{(*)}}$ and $\lambda_{\phi^{(*)}}$ represent mixing constants with $\lambda_{S_3} = \lambda_{S_3^*}$, $\lambda_{S_1} = \lambda_{S_1^*}$ and $\lambda_\phi = \lambda_{\phi^*}$, since h is a real field. According to Eq. (19), Feynman rule of $U_{1\mu}U_{1\nu}^*h$ should be expressed as

$$U_{1\mu}U_{1\nu}^*h : \frac{i}{2}g_4^2 \left(\frac{v_3}{2\sqrt{3}}\lambda_{S_3} + \frac{v_1}{\sqrt{2}}\lambda_{S_1} \right) g_{\mu\nu}. \quad (26)$$

We do not intend to further solve these mixing parameters $\lambda_{S_{3,1}^{(*)}}$. For convenience, we re-express the Feynman rule as

$$U_{1\mu}U_{1\nu}^*h : \frac{i}{2}g_4^2 v g_{\mu\nu} \frac{v_3}{v} \lambda_V, \quad (27)$$

where the U_1 -Higgs coupling $\lambda_V = \frac{\lambda_{S_3}}{2\sqrt{3}} + \frac{v_1}{v_3} \frac{\lambda_{S_1}}{\sqrt{2}}$, which is expected to be small according to current Higgs measurements analyses in Section 2.

We now consider interactions among gauge bosons. The interactions are obtained from the gauge kinetic term [31]

$$\mathcal{L}_{gauge} = -\frac{1}{4}H_{\mu\nu}^\alpha H^{\alpha,\mu\nu} - \frac{1}{4}G_{\mu\nu}^a G'^{a,\mu\nu} - \frac{1}{4}W_{\mu\nu}^i W^{i,\mu\nu} - \frac{1}{4}B'_{\mu\nu} B'^{\mu\nu}, \quad (28)$$

where definitions of field strengths $H_{\mu\nu}^\alpha$, $G_{\mu\nu}^{\prime a}$, $W_{\mu\nu}^i$ and $B'_{\mu\nu}$ see [31].

Prior to electroweak symmetry breaking, the massless $SU(3)_c \times U(1)_Y$ degrees of freedom of \mathcal{G}_{SM} expressed in terms of the original gauge fields are given by [31]

$$g_\mu^a = \frac{g_3 H_\mu^a + g_4 G_\mu^{\prime a}}{\sqrt{g_4^2 + g_3^2}}, \quad (29)$$

$$B_\mu = \frac{\sqrt{\frac{2}{3}}g_1 H_\mu^{15} + g_4 B'_\mu}{\sqrt{g_4^2 + \frac{2}{3}g_1^2}}. \quad (30)$$

The SM gauge couplings are matched as [31]

$$g_s = \frac{g_4 g_3}{\sqrt{g_4^2 + g_3^2}}, \quad (31)$$

$$g_Y = \frac{g_4 g_1}{\sqrt{g_4^2 + \frac{2}{3}g_1^2}}. \quad (32)$$

Then, one can obtain Feynman rules related to U_1 interactions to the SM gauge boson γ and g ,

$$\begin{pmatrix} U_{1\mu}(k_1) \\ U_{1\nu}^*(k_2) \\ A_\rho(k_3) \end{pmatrix} : -i \frac{\frac{2}{3}g_4 g_1 \cos(\theta_W)}{\sqrt{g_4^2 + \frac{2}{3}g_1^2}} V_{\mu\nu\rho}(k_1, k_2, k_3) = -ie Q_U V_{\mu\nu\rho}(k_1, k_2, k_3), \quad (33)$$

$$\begin{pmatrix} U_{1\mu}(k_1) \\ U_{1\nu}^*(k_2) \\ A_\rho(k_3) \\ A_\sigma(k_4) \end{pmatrix} : i(eQ_U)^2 (g_{\mu\rho}g_{\nu\sigma} + g_{\mu\sigma}g_{\nu\rho} - 2g_{\mu\nu}g_{\rho\sigma}), \quad (34)$$

$$\begin{pmatrix} U_{1\mu}^i(k_1) \\ U_{1\nu}^{*j}(k_2) \\ g_\rho^a(k_3) \end{pmatrix} : -i \frac{g_4 g_3}{\sqrt{g_4^2 + g_3^2}} T_{ij}^a V_{\mu\nu\rho}(k_1, k_2, k_3) = -ig_s T_{ij}^a V_{\mu\nu\rho}(k_1, k_2, k_3), \quad (35)$$

$$\begin{pmatrix} U_{1\mu}^i(k_1) \\ U_{1\nu}^{*j}(k_2) \\ g_\rho^a(k_3) \\ g_\sigma^b(k_4) \end{pmatrix} : ig_s^2 \delta_{ij} \frac{\delta_{ab}}{4} (g_{\mu\rho}g_{\nu\sigma} + g_{\mu\sigma}g_{\nu\rho} - 2g_{\mu\nu}g_{\rho\sigma}), \quad (36)$$

where θ_W is the Weinberg angle, the function $V_{\mu\nu\rho}(k_1, k_2, k_3)$ is defined as

$$V_{\mu\nu\rho}(k_1, k_2, k_3) = g_{\mu\nu}(k_2 - k_1)_\rho + g_{\nu\rho}(k_3 - k_2)_\mu - g_{\rho\mu}(k_1 - k_3)_\nu,$$

with k_i being four-momentum of the i -th particle (direction towards the vertex is specified to be positive).

4.2 Constraints on U_1 from Higgs data

By using Eqs. (27,33-36), we obtain the partial decay width of $h \rightarrow \gamma\gamma$ and cross section of $gg \rightarrow h$ in presence of U_1

$$\Gamma(h \rightarrow \gamma\gamma) = \frac{G_F \alpha_{em}^2 m_h^3}{128\sqrt{2}\pi^3} \left| F_1(x_W) + \frac{4}{3}F_{1/2}(x_t) + \xi_V d(r_U) Q_U^2 F_1(x_U) \right|^2, \quad (37)$$

and

$$\sigma_0 = \frac{G_F \alpha_s^2(\mu^2)}{512\sqrt{2}\pi} \left| F_{1/2}(x_t) + \xi_V F_1(x_U) \right|^2, \quad (38)$$

where

$$\xi_V = \frac{g_4^2 \lambda_V v v_3}{4m_U^2} = \frac{\lambda_V v v_3}{v_3^2 + v_1^2}. \quad (39)$$

In obtaining Eq. (39), we have used mass expression Eq. (17). Eq. (39) shows that the '4321' model's U_1 modifications to the loop-induced Higgs processes depend on U_1 -Higgs coupling λ_V and new VEVs v_3 and v_1 in the model rather than the mass of U_1 and gauge coupling g_4 . This means that once ξ_V is determined from the Higgs fit one can determine v_3 and v_1 by using ξ_V together with other condition such as the mass of U_1 determined from colliders.

For single vector LQ U_1 modifying partial decay width of $h \rightarrow \gamma\gamma$ and cross section of $gg \rightarrow h$, coupling modifiers κ_γ and κ_g are expressed with ξ_V , which read

$$\kappa_\gamma = 1 + 1.44\xi_V \text{ and } \kappa_g = 1 - 5.09\xi_V. \quad (40)$$

To obtain the size of U_1 interaction with the Higgs boson, we re-analyze the Higgs data by using Eq. (40). The best value with standard error and 95% C.L. intervals of ξ_V obtained from the Higgs fit are

$$\xi_V = -0.005 \pm 0.008, \quad (41)$$

and

$$\xi_V \in [-0.021, 0.011]. \quad (42)$$

For U_1 -Higgs coupling with value of one-third (-tenth) of the electromagnetic coupling strength, $|\lambda_V| = 0.1(0.03)$, ξ_V varying as a function of v_3 for a fixed value of v_1 and combined limits on v_3 and v_1 from the condition, $v_3 > v_1 > v$, as well as current Higgs data, are shown in Fig. 2. From Fig. 2 one can see that we still need more precise Higgs measurements, since at least the sign of λ_V has not been determined yet from current Higgs data. It should be noted that the result of precision on ξ_S is also applicable to ξ_V , which means the precision on ξ_V is expected to improve by a factor of 2.4 compared with present situation at HL-LHC.

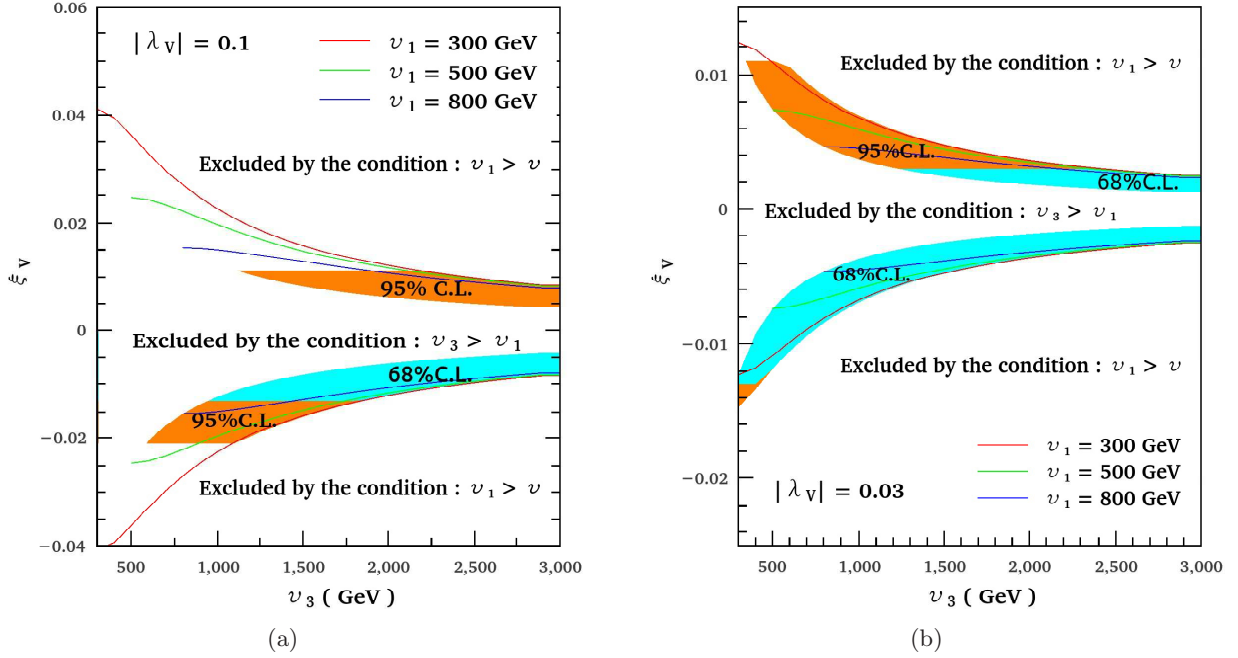


Figure 2: Limits on v_3 and v_1 from combination of phenomenological condition, $v_3 > v_1 > v$, and constraints from Higgs fit. The cyan region is allowed at 68% C.L. from the Higgs fit while the orange area is allowed at 95% C.L.. The coupling size is assumed with value of (a) $|\lambda_V| = 0.1$ and (b) $|\lambda_V| = 0.03$. The red (green, orange) line represents ξ_V varying as a function of v_3 , in assuming v_1 with fixed value of 300 (500, 800) GeV.

4.3 Combined limits on the relation of λ_V and $v_{3,1}$

We can further constrain the relation of λ_V and $v_{3,1}$ by combined limits on ξ_V obtained in this analysis and m_U obtained from direct searches at colliders as well as measurements of $R_{D^{(*)}}$ and $R_{K^{(*)}}$. Details of obtaining the constraints on U_1 from B -anomalies are shown in appendix A

Current lower limits on masses of vector LQs with decay mode $LQ \rightarrow t\nu/b\tau$ is $m_{LQ} > 1530$ GeV reported by the CMS collaboration [78]. For $g_4 = 3.5$,

$$v_3^2 + v_1^2 = \frac{4}{g_4^2} m_U^2 > (874 \text{ GeV})^2, \quad (43)$$

which is looser than the constraints from B -anomalies. Thus we consider combined constraints from the LHC Higgs data and B -anomalies measurements, which is performed via minimizing

$$\chi^2 = \chi_{\text{Higgs}}^2 + \chi_B^2, \quad (44)$$

where χ_{Higgs}^2 has been shown in Eq. (2) and χ_B^2 is explained in Eq. (66). Assuming tree level contributions induced by U_1 dominant the NP contributions to B -anomalies. Fig. 3 shows two dimensional likelihood contours at 68% and 95% C.L. in $(v_3^2 + v_1^2, \lambda_V v_3)$ plane obtained from combination of the LHC Higgs data together with measurements of B -anomalies. Best values of $v_3^2 + v_1^2$ and $\lambda_V v_3$ read

$$v_3^2 + v_1^2 = 1.496 \pm 0.250 \text{ TeV}^2 \text{ and } \lambda_V v_3 = -0.0315 \pm 0.0473 \text{ TeV}. \quad (45)$$

Assuming $\lambda_V = -0.1(-0.03)$, we show the constraints on $v_{3,1}$ in Fig. 4, which are obtained from combined limits of LHC Higgs data and B -anomalies as well as the condition $v_3 > v_1 > v$. The best value of v_3 obtained under the assumption of $\lambda_V = -0.1$ does not in the allowed region as shown in Fig. 4 (a), while that does for $\lambda_V = -0.03$ (see Fig. 4 (b)).

If the Higgs coupling and $R_{D^{(*)}}$ and $R_{K^{(*)}}$ precisely measured in the future, we can determine VEVs v_3 and v_1 . For $\lambda_V = -0.03$, at the best fit value point, we obtain

$$v_3 = 1.051 \text{ TeV and } v_1 = 0.625 \text{ TeV}. \quad (46)$$

Equivalently, we obtain the mass of U_1

$$m_U = \frac{1}{2} g_4 \sqrt{v_3^2 + v_1^2} = 2.140 \text{ TeV} \quad (47)$$

Then, one can determine or constrain other parameters in the model directly by using $v_3 = 1.051$ GeV and $v_1 = 0.625$ GeV, or together with other constraints. For example, we can directly determine the masses of the other two new gauge particles g' and Z' in the model [31]. Assuming $g_4 = 3.5$ and $g_3 = 1.07$ as well as $g_1 = 0.364$, we obtain

$$m_{g'} = \sqrt{\frac{1}{2}(g_4^2 + g_3^2)v_3^2} = 2.72 \text{ TeV}, \quad (48)$$

$$m_{Z'} = \sqrt{\frac{1}{4}\left(\frac{3}{2}g_4^2 + g_1^2\right)\left(\frac{1}{3}v_3^2 + v_1^2\right)} = 1.88 \text{ TeV}. \quad (49)$$

Alternatively, once two of the three massive particles U_1 , g' and Z' are found at the LHC or future colliders, one can use these masses together with ξ_V to determine the U_1 -Higgs coupling λ_V .

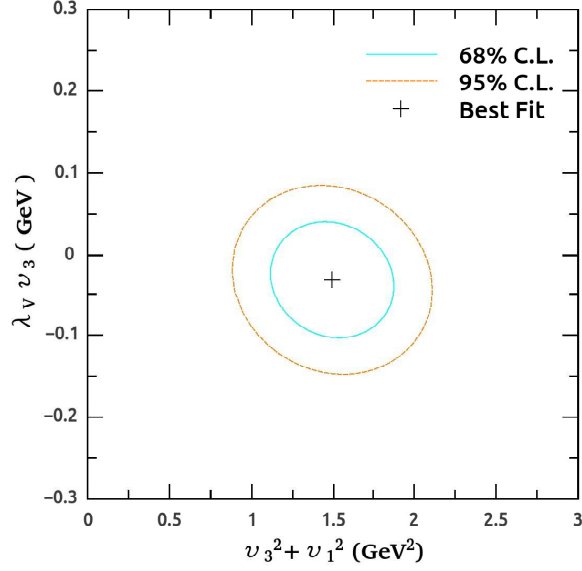


Figure 3: Two dimensional likelihood contours at 68% and 95% C.L. in $(v_3^2 + v_1^2, \lambda_V v_3)$ plane obtained from combined limits of the LHC Higgs data together with constraints from B -anomalies measurements. The cross is the best-fit value.

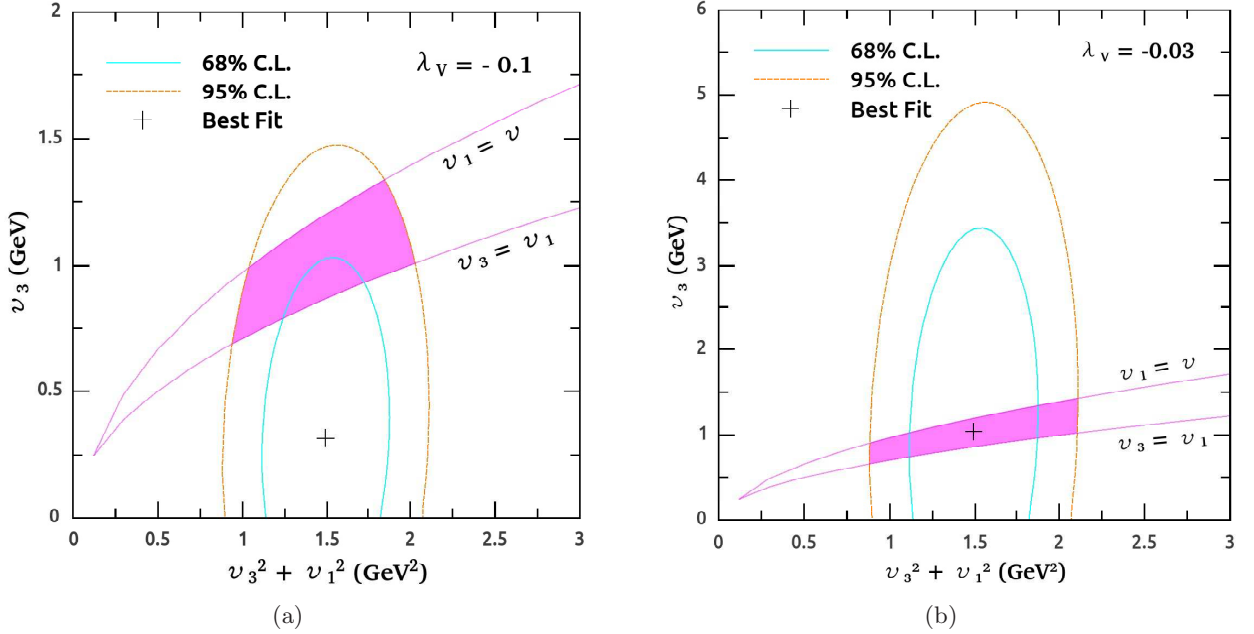


Figure 4: Limits on v_3 and v_1 from combination of Higgs fit and B -anomalies measurements as well as phenomenological condition, $v_3 > v_1 > v$. The U_1 coupling is assumed with value of (a) $\lambda_V = -0.1$ and (b) $\lambda_V = -0.03$. The LQ is survived in the pink regions.

5 Conclusions

B -anomalies may be a long-awaited new physical signal, and is discussed extensively as a hot topic. The good performance in explaining B -anomalies indicates that LQ may be discovered in the near future.

LQs with mass value of TeV-scale can considerably modify loop-induced Higgs processes, ggF production and $h \rightarrow \gamma\gamma$ decay, which depending on the coupling size of LQ interactions with the Higgs boson. We study contributions of single scalar or vector LQ to loop-induced Higgs processes by analyzing current LHC Higgs data. Scalar LQs are studied model-independently while vector LQ, $U_1(\mathbf{3}, \mathbf{1}, 2/3)$, is discussed in so called the '4321' model.

Constraints on sizes of portal interactions, $\lambda_S = \lambda_S(v/m_S)^2$, of all possible scalar LQs are obtained. Currently, the constraints for all scalar LQs are still too loose to acquire exact information for scalar LQ with mass of TeV scale, although accuracy of the result in this analysis is more than doubled compared with previous one by analyzing Higgs data from LHC Run I [53].

For vector LQ, $U_1(\mathbf{3}, \mathbf{1}, 2/3)$, the size of interaction between U_1 and Higgs boson is parameterized as

$$\xi_V = \frac{\lambda_V v v_3}{v_3^2 + v_1^2},$$

where λ_V is the U_1 -Higgs coupling constant. The best value with standard error and 95% C.L. intervals for ξ_V obtained from the Higgs fit read

$$\xi_V = -0.005 \pm 0.008, \quad \xi_V \in [-0.021, 0.011].$$

The LQ coupling λ_V is constrained to be small (< 0.3) for TeV-scale mass U_1 , which is in accordance with the prediction of the '4321' model.

Compared to the present precision on $\xi_{S(V)}$, the situation is expected to improve by a factor of 2.4 at the HL-LHC.

We provide a method to determine VEVs, v_3 and v_1 , of new scalar fields, Ω_3 and Ω_1 in the '4321' model, via the combination of the relation $\xi_V = \lambda_V v v_3 / (v_3^2 + v_1^2)$ together with direct searches of U_1 at colliders as well as other constraints such as measurements of $R_{D^{(*)}}$ and $R_{K^{(*)}}$.

For conclusion, loop-induced Higgs processes ggF production and $h \rightarrow \gamma\gamma$ decay are important processes that contributions of new heavy particles such as LQs may hidden in. We expect more precise measurements of Higgs properties in the future to guide us in the direction for LQ study.

Acknowledgements

We thank Ilja Doršner for discussions. This work is supported in part by the National Natural Science Foundation of China under Grants No.11875157 and 11847303 (C. X. Yue and J. Zhang), and Liaoning Revitalization Talents Program No.60618009 (C. H. Li).

A

Contributions of U_1 to $R_{D^{(*)}}$ and $R_{K^{(*)}}$

For the charged current $b \rightarrow c\ell\nu$, U_1 modifies $R_{D^{(*)}} = \frac{\mathcal{B}(\bar{B} \rightarrow D^{(*)}\tau^-\bar{\nu})}{\mathcal{B}(\bar{B} \rightarrow D^{(*)\ell}\bar{\nu})}$ ($\ell = e, \mu$) by [31]

$$\begin{aligned} \Delta R_{D^{(*)}} &= \frac{R_{D^{(*)}}^{\text{exp}}}{R_{D^{(*)}}^{\text{SM}}} - 1 \\ &\approx 0.2 \left(\frac{2 \text{ TeV}}{m_U} \right)^2 \left(\frac{g_4}{3.5} \right)^2 \sin(2\theta_{LQ}) \left(\frac{s_{\ell_3}}{0.8} \right)^2 \left(\frac{s_{q_3}}{0.8} \right) \left(\frac{s_{q_2}}{0.35} \right). \end{aligned} \quad (50)$$

Setting $\theta_{LQ} = \pi/4$, $s_{\ell_3} = s_{q_3} = 0.8$, $s_{q_2} = 0.35$ and $g_4 = 3.5$, we obtain

$$\Delta R_{D^{(*)}} \approx 0.2 \left(\frac{2000 \text{ GeV}}{m_U} \right)^2 \approx 0.2 \frac{(1143 \text{ GeV})^2}{v_3^2 + v_1^2}. \quad (51)$$

For neutral currents $b \rightarrow s\ell\ell$ case, U_1 's tree level contributions to Wilson coefficients $C_9^{\mu\mu}$ and $C_{10}^{\mu\mu}$ ($C_i = C_i^{\text{SM}} + \Delta C_i$) in the '4321' model are given by [31]

$$\Delta C_9^{\mu\mu}|_{\text{tree}} = -\Delta C_{10}^{\mu\mu}|_{\text{tree}} = \frac{2\pi}{\alpha_{em} V_{tb} V_{ts}^*} C_U \beta_{s\mu} \beta_{b\mu}^*, \quad (52)$$

where $C_U = g_4^2 v^2 / (4m_U^2)$, $\beta_{s\mu} = c_{\theta_{LQ}} s_{q_2} s_{\ell_2}$, $\beta_{b\mu} = -s_{\theta_{LQ}} s_{q_3} s_{\ell_2}$. For $\theta_{LQ} = \pi/4$, $s_{\ell_2} = 0.06$, $s_{q_3} = 0.8$, $s_{q_2} = 0.35$ and $g_4 = 3.5$, we obtain

$$\Delta C_9^{\mu\mu}|_{\text{tree}} = -\Delta C_{10}^{\mu\mu}|_{\text{tree}} = -0.46 \frac{(1143 \text{ GeV})^2}{v_3^2 + v_1^2} \quad (53)$$

One-loop log-enhanced processes at the scale of the bottom mass may also contribute to the neutral currents sizeable. The contribution of the loops only to $C_9^{\ell\ell}$, which, in the $\beta_{b\tau}|V_{ts}| \ll \beta_{s\tau}$ limit, is given by [31]

$$\Delta C_9^{\ell\ell}|_{\text{loop}}(m_b^2) \approx \frac{1}{3} \Delta R_{D^{(*)}} \left(\log x_b - \frac{1}{s_\tau^2} \log x_{E_2} \right), \quad (54)$$

where $x_\alpha = m_\alpha^2/m_U^2$, E_2 is a vector-like lepton introduced in the model. The contribution is universal for all leptons. Taking Eq. (51) in to the above equation and setting $s_\tau = 0.8$, $m_{E_2} = 850 \text{ GeV}$, we have

$$\Delta C_9^{\ell\ell}|_{\text{loop}}(m_b^2) \approx \frac{0.2}{3} \frac{(1143 \text{ GeV})^2}{v_3^2 + v_1^2} \left(\log \frac{(4.8 \times 10^{-3} \text{ TeV})^2}{v_3^2 + v_1^2} - \frac{1}{0.8^2} \log \frac{(0.97 \text{ TeV})^2}{v_3^2 + v_1^2} \right). \quad (55)$$

Thus U_1 modifies the $b \rightarrow s\ell\ell$ processes via

$$\delta C_9^{\mu\mu} = \Delta C_{9,U_1}^{\mu\mu}|_{\text{tree}} + \Delta C_{9,U_1}^{\mu\mu}|_{\text{loop}}, \quad (56)$$

$$\delta C_{10}^{\mu\mu} = -\Delta C_{9,U_1}^{\mu\mu}|_{\text{tree}}, \quad (57)$$

$$\delta C_9^{ee} = \Delta C_{9,U_1}^{\mu\mu}|_{\text{loop}}, \quad (58)$$

$$\delta C_{10}^{ee} = 0. \quad (59)$$

In this analysis, we consider the U_1 contributions to $b \rightarrow s\ell\ell$ processes in the case of

scenario A. only via tree level contributions (Eq. (53)), i.e.

$$\begin{aligned}\delta C_9^{\mu\mu} &= -\delta C_{10}^{\mu\mu} = \Delta C_{9,U_1}^{\mu\mu} \Big|_{\text{tree}}, \\ \delta C_9^{ee} &= \delta C_{10}^{ee} = 0.\end{aligned}\tag{60}$$

scenario B. only via loop contributions (Eq. (54)), i.e.

$$\begin{aligned}\delta C_9^{\mu\mu} &= \delta C_9^{ee} = \Delta C_{9,U_1}^{\mu\mu} \Big|_{\text{loop}}, \\ \delta C_{10}^{\mu\mu} &= \delta C_{10}^{ee} = 0.\end{aligned}\tag{61}$$

Fit to $R_{D^{(*)}}$ and $R_{K^{(*)}}$ measurements

The newest average values of R_D and R_{D^*} including preliminary results at Belle II experiment [80] are given by [79]

$$R_D = 0.337 \pm 0.030 \quad \text{and} \quad R_{D^*} = 0.299 \pm 0.013,\tag{62}$$

with a correlation of -0.36. The SM predictions of these two measurements read

$$R_D^{SM} = 0.300_{-0.004}^{+0.005} \quad \text{and} \quad R_{D^*}^{SM} = 0.251_{-0.003}^{+0.004}.\tag{63}$$

Then we obtain

$$\Delta R_D = 0.123 \pm 0.101 \quad \text{and} \quad \Delta R_{D^*} = 0.191 \pm 0.054,\tag{64}$$

the correlation between the two quantities reads -0.34.

Ref. [81] has updated the $b \rightarrow s$ anomalies by including newest measurements of R_K measured by the LHCb collaboration [82], R_{K^*} measured by the Belle collaboration [83] as well as $B_{s,d} \rightarrow \mu^+\mu^-$ measured by the ATLAS collaboration [84]. The best fit values of $\Delta C_{9,U_1}^{\mu\mu} \Big|_{\text{tree}}$ and $\Delta C_{9,U_1}^{\mu\mu} \Big|_{\text{loop}}$ read respectively

$$\Delta C_{9,U_1}^{\mu\mu} \Big|_{\text{tree}} = -0.41 \pm 0.10 \quad \text{and} \quad \Delta C_{9,U_1}^{\mu\mu} \Big|_{\text{loop}} = -1.01 \pm 0.20.\tag{65}$$

To obtain $v_3^2 + v_1^2$, we perform our fit to measurements in Eqs. (64) and (65) by minimizing

$$\chi_B^2 = \left(\Delta R^{exp} - \Delta R^{the} \right) C_{\Delta R}^{-1} \left(\Delta R^{exp} - \Delta R^{the} \right) + \frac{(\Delta C_9^{exp} - \Delta C_9^{the})^2}{(\delta C_9^{\mu\mu})^2},\tag{66}$$

where ΔR^{exp} denotes the measurement of $\Delta R_{D^{(*)}}$ and ΔR^{the} represents its theoretical prediction as shown in Eq. 51. Similarly, $\Delta C_9^{\mu\mu,exp}$ denotes $\Delta C_9^{\mu\mu}$ measured at experiments and $\Delta C_9^{\mu\mu,the}$ is its theoretical prediction as shown in Eq. 53 or Eq. 54.

Then, we obtain the best fit value and preferred 95% C.L. intervals of $v_3^2 + v_1^2$, for the case of scenario **A**

$$v_3^2 + v_1^2 = 1.496 \pm 0.250 \text{ TeV}^2, \quad (67)$$

$$v_3^2 + v_1^2 \in [1.127, 2.226] \text{ TeV}^2 \text{ at } 95\% \text{C.L.}, \quad (68)$$

for the case of scenario **B**

$$v_3^2 + v_1^2 = 1.220 \pm 0.187 \text{ TeV}^2, \quad (69)$$

$$v_3^2 + v_1^2 \in [0.939, 1.748] \text{ TeV}^2 \text{ at } 95\% \text{C.L.}. \quad (70)$$

References

- [1] R. Aaij *et al.* [LHCb Collaboration], Phys. Rev. Lett. **113** (2014) 151601 [arXiv:1406.6482 [hep-ex]].
- [2] R. Aaij *et al.* [LHCb Collaboration], JHEP **1708** (2017) 055 [arXiv:1705.05802 [hep-ex]].
- [3] M. Bordone, G. Isidori and A. Pattori, Eur. Phys. J. C **76** (2016) no.8, 440 [arXiv:1605.07633 [hep-ph]].
- [4] B. Capdevila, S. Descotes-Genon, L. Hofer and J. Matias, JHEP **1704** (2017) 016 [arXiv:1701.08672 [hep-ph]].
- [5] R. Aaij *et al.* [LHCb Collaboration], Phys. Rev. Lett. **115** (2015) no.11, 111803 Erratum: [Phys. Rev. Lett. **115** (2015) no.15, 159901] [arXiv:1506.08614 [hep-ex]].
- [6] M. Huschle *et al.* [Belle Collaboration], Phys. Rev. D **92** (2015) no.7, 072014 [arXiv:1507.03233 [hep-ex]].
- [7] Y. Sato *et al.* [Belle Collaboration], Phys. Rev. D **94** (2016) no.7, 072007 [arXiv:1607.07923 [hep-ex]].
- [8] S. Hirose *et al.* [Belle Collaboration], Phys. Rev. Lett. **118** (2017) no.21, 211801 [arXiv:1612.00529 [hep-ex]].
- [9] J. P. Lees *et al.* [BaBar Collaboration], Phys. Rev. Lett. **109** (2012) 101802 [arXiv:1205.5442 [hep-ex]].
- [10] J. P. Lees *et al.* [BaBar Collaboration], Phys. Rev. D **88** (2013) no.7, 072012 [arXiv:1303.0571 [hep-ex]].
- [11] Heavy Flavor Averaging Group, Average of R_D and R_D^* for FPCP 2017, <http://www.slac.stanford.edu/xorg/hfag/semi/fpcp17/RDRDs.html> (2017).
- [12] S. Fajfer, J. F. Kamenik and I. Nisandzic, Phys. Rev. D **85** (2012) 094025 [arXiv:1203.2654 [hep-ph]].
- [13] S. Aoki *et al.*, Eur. Phys. J. C **77** (2017) no.2, 112 [arXiv:1607.00299 [hep-lat]].
- [14] B. Gripaios, M. Nardecchia and S. A. Renner, JHEP **1505** (2015) 006 [arXiv:1412.1791 [hep-ph]].

- [15] H. Georgi and Y. Nakai, Phys. Rev. D **94** (2016) no.7, 075005 [arXiv:1606.05865 [hep-ph]].
- [16] D. Bečirević, S. Fajfer, N. Košnik and O. Sumensari, Phys. Rev. D **94** (2016) no.11, 115021 [arXiv:1608.08501 [hep-ph]].
- [17] D. Bečirević and O. Sumensari, JHEP **1708** (2017) 104 [arXiv:1704.05835 [hep-ph]].
- [18] B. Diaz, M. Schmaltz and Y. M. Zhong, JHEP **1710** (2017) 097 [arXiv:1706.05033 [hep-ph]].
- [19] D. Buttazzo, A. Greljo, G. Isidori and D. Marzocca, JHEP **1711** (2017) 044 [arXiv:1706.07808 [hep-ph]].
- [20] S. Y. Guo, Z. L. Han, B. Li, Y. Liao and X. D. Ma, Nucl. Phys. B **928** (2018) 435 [arXiv:1707.00522 [hep-ph]].
- [21] L. Di Luzio, A. Greljo and M. Nardecchia, Phys. Rev. D **96** (2017) no.11, 115011 [arXiv:1708.08450 [hep-ph]].
- [22] L. Calibbi, A. Crivellin and T. Li, Phys. Rev. D **98** (2018) no.11, 115002 [arXiv:1709.00692 [hep-ph]].
- [23] M. Blanke and A. Crivellin, Phys. Rev. Lett. **121** (2018) no.1, 011801 [arXiv:1801.07256 [hep-ph]].
- [24] S. Fajfer, N. Košnik and L. Vale Silva, Eur. Phys. J. C **78** (2018) no.4, 275 [arXiv:1802.00786 [hep-ph]].
- [25] S. Matsuzaki, K. Nishiwaki and K. Yamamoto, JHEP **1811** (2018) 164 [arXiv:1806.02312 [hep-ph]].
- [26] C. Hati, G. Kumar, J. Orloff and A. M. Teixeira, JHEP **1811** (2018) 011 [arXiv:1806.10146 [hep-ph]].
- [27] D. Bečirević, I. Doršner, S. Fajfer, N. Košnik, D. A. Faroughy and O. Sumensari, Phys. Rev. D **98** (2018) no.5, 055003 [arXiv:1806.05689 [hep-ph]].
- [28] A. Crivellin, C. Greub, D. Müller and F. Saturnino, Phys. Rev. Lett. **122** (2019) no.1, 011805 [arXiv:1807.02068 [hep-ph]].
- [29] I. de Medeiros Varzielas and S. F. King, JHEP **1811** (2018) 100 [arXiv:1807.06023 [hep-ph]].
- [30] A. Azatov, D. Barducci, D. Ghosh, D. Marzocca and L. Ubaldi, JHEP **1810** (2018) 092 [arXiv:1807.10745 [hep-ph]].
- [31] L. Di Luzio, J. Fuentes-Martin, A. Greljo, M. Nardecchia and S. Renner, JHEP **1811** (2018) 081 [arXiv:1808.00942 [hep-ph]].
- [32] T. Faber, M. Hudec, M. Malinský, P. Meinzinger, W. Porod and F. Staub, Phys. Lett. B **787** (2018) 159 [arXiv:1808.05511 [hep-ph]].
- [33] J. Heeck and D. Teresi, JHEP **1812** (2018) 103 [arXiv:1808.07492 [hep-ph]].
- [34] A. Angelescu, D. Bečirević, D. A. Faroughy and O. Sumensari, JHEP **1810** (2018) 183 [arXiv:1808.08179 [hep-ph]].

- [35] S. Balaji, R. Foot and M. A. Schmidt, Phys. Rev. D **99** (2019) no.1, 015029 [arXiv:1809.07562 [hep-ph]].
- [36] R. Watanabe, arXiv:1810.00379 [hep-ph].
- [37] M. Schmaltz and Y. M. Zhong, JHEP **1901** (2019) 132 [arXiv:1810.10017 [hep-ph]].
- [38] S. Bansal, R. M. Capdevilla and C. Kolda, Phys. Rev. D **99** (2019) no.3, 035047 [arXiv:1810.11588 [hep-ph]].
- [39] S. Iguro, T. Kitahara, Y. Omura, R. Watanabe and K. Yamamoto, JHEP **1902** (2019) 194 [arXiv:1811.08899 [hep-ph]].
- [40] S. Fajfer, EPJ Web Conf. **192** (2018) 00025.
- [41] B. Fornal, S. A. Gadam and B. Grinstein, Phys. Rev. D **99** (2019) no.5, 055025 [arXiv:1812.01603 [hep-ph]].
- [42] L. Da Rold and F. Lamagna, JHEP **1903** (2019) 135 [arXiv:1812.08678 [hep-ph]].
- [43] I. de Medeiros Varzielas and J. Talbert, arXiv:1901.10484 [hep-ph].
- [44] J. Zhang, Y. Zhang, Q. Zeng and R. Sun, Eur. Phys. J. C **79** (2019) no.2, 164.
- [45] U. Aydemir, T. Mandal and S. Mitra, arXiv:1902.08108 [hep-ph].
- [46] O. Catà and T. Mannel, arXiv:1903.01799 [hep-ph].
- [47] B. Bhattacharya, A. Datta, S. Kamali and D. London, arXiv:1903.02567 [hep-ph].
- [48] A. S. Adam, A. Ferdiyana and M. Satriawan, arXiv:1903.03370 [hep-ph].
- [49] J. Aebischer, W. Altmannshofer, D. Guadagnoli, M. Reboud, P. Stangl and D. M. Straub, arXiv:1903.10434 [hep-ph].
- [50] C. Cornella, J. Fuentes-Martin and G. Isidori, arXiv:1903.11517 [hep-ph].
- [51] R. Barbieri and R. Ziegler, arXiv:1904.04121 [hep-ph].
- [52] W. Buchmuller, R. Ruckl and D. Wyler, Phys. Lett. B **191** (1987) 442 Erratum: [Phys. Lett. B **448** (1999) 320].
- [53] I. Doršner, S. Fajfer, A. Greljo, J. F. Kamenik and N. Košnik, Phys. Rept. **641** (2016) 1 [arXiv:1603.04993 [hep-ph]].
- [54] M. Tanabashi *et al.* [Particle Data Group], Phys. Rev. D **98** (2018) no.3, 030001.
- [55] J. C. Pati and A. Salam, Phys. Rev. D **10** (1974) 275. Erratum: [Phys. Rev. D **11** (1975) 703].
- [56] H. Georgi and S. L. Glashow, Phys. Rev. Lett. **32** (1974) 438.
- [57] H. Georgi, AIP Conf. Proc. **23** (1975) 575.
- [58] B. Schrempp and F. Schrempp, Phys. Lett. **153B**, 101 (1985).

- [59] J. Wudka, Phys. Lett. **167B** (1986) 337.
- [60] I. Doršner, S. Fajfer, A. Greljo, J. F. Kamenik, N. Košnik and I. Nišandžic, JHEP **1506** (2015) 108 [arXiv:1502.07784 [hep-ph]].
- [61] W. F. Chang, J. N. Ng and J. M. S. Wu, Phys. Rev. D **86** (2012) 033003 [arXiv:1206.5047 [hep-ph]].
- [62] G. Aad *et al.* [ATLAS Collaboration], JINST **3** (2008) S08003.
- [63] S. Chatrchyan *et al.* [CMS Collaboration], JINST **3** (2008) S08004.
- [64] G. Aad *et al.* [ATLAS and CMS Collaborations], JHEP **1608** (2016) 045 [arXiv:1606.02266 [hep-ex]].
- [65] The ATLAS collaboration [ATLAS Collaboration], ATLAS-CONF-2019-005.
- [66] A. M. Sirunyan *et al.* [CMS Collaboration], Submitted to: Eur.Phys.J. [arXiv:1809.10733 [hep-ex]].
- [67] The ATLAS and CMS Collaborations, ATLAS-CONF-2015-044.
- [68] CMS Collaboration [CMS Collaboration], CMS-PAS-HIG-15-002.
- [69] S. Heinemeyer *et al.* [LHC Higgs Cross Section Working Group], arXiv:1307.1347 [hep-ph].
- [70] T. Enkhbat, JHEP **1401** (2014) 158 [arXiv:1311.4445 [hep-ph]].
- [71] A. Djouadi, Phys. Rept. **459** (2008) 1 [hep-ph/0503173].
- [72] M. Carena, I. Low and C. E. M. Wagner, JHEP **1208** (2012) 060 [arXiv:1206.1082 [hep-ph]].
- [73] I. Dorsner, S. Fajfer, A. Greljo and J. F. Kamenik, JHEP **1211** (2012) 130 [arXiv:1208.1266 [hep-ph]].
- [74] P. Agrawal and U. Mahanta, Phys. Rev. D **61** (2000) 077701 [hep-ph/9911497].
- [75] S. Gori and I. Low, JHEP **1309** (2013) 151 [arXiv:1307.0496 [hep-ph]].
- [76] M. Aaboud *et al.* [ATLAS Collaboration], arXiv:1902.00377 [hep-ex].
- [77] M. Cepeda *et al.* [Physics of the HL-LHC Working Group], arXiv:1902.00134 [hep-ph].
- [78] A. M. Sirunyan *et al.* [CMS Collaboration], Phys. Rev. D **98** (2018) no.3, 032005 [arXiv:1805.10228 [hep-ex]].
- [79] C. Murgui, A. Peñuelas, M. Jung and A. Pich, arXiv:1904.09311 [hep-ph].
- [80] A. Abdesselam *et al.* [Belle Collaboration], arXiv:1904.08794 [hep-ex].
- [81] A. Arbey, T. Hurth, F. Mahmoudi, D. Martinez Santos and S. Neshatpour, arXiv:1904.08399 [hep-ph].
- [82] R. Aaij *et al.* [LHCb Collaboration], arXiv:1903.09252 [hep-ex].

- [83] A. Abdesselam *et al.* [Belle Collaboration], arXiv:1904.02440 [hep-ex].
- [84] M. Aaboud *et al.* [ATLAS Collaboration], JHEP **1904** (2019) 098 doi:10.1007/JHEP04(2019)098 [arXiv:1812.03017 [hep-ex]].